15. H. H. Demarest, Jr., "Hugoniot curves and the Grüneisen parameters at high pressure for the alkali halides," J. Phys. Chem. Solids, 35, 1393 (1974).

SHOCK WAVES AND PHASE TRANSITIONS IN IRON

N. Kh. Akhmadeev and R. I. Nigmatulin

UDC 539.89

INTRODUCTION

The process of shock compression in certain solids (iron, carbon, KCl, KBr, quartz, many minerals) is accompanied at increased pressure p_S by phase transitions, i.e., formation of new crystalline phases [1]. Changes in the wave configurations which then develop [2-4] permit determination of the characteristic times of these transitions, which usually comprise 0.2-0.4 μsec. In [5-7] a single-velocity single-temperature model of a two-phase viscoplastic medium was developed, which was used for study of nonstationary shock waves in Armco iron with phase transitions, and on the basis of the relationship between phase transitions and hardening, the kinetics of the phase transition $\alpha \rightleftharpoons \varepsilon$ in iron were determined. In the present study an investigation of shock-wave propagation in Armco iron will be performed with consideration of new experiments [3, 4] in which the multiwave structure of shock waves of various intensities were fixed directly by manganin sensors and a light interferometer. Under these experimental conditions, calculations were performed for motion of shock waves on the front of which phase transitions occur. The kinetics of phase transition will be studied and presented in greater detail than in [6, 7].

§1. The basic equations in Lagrangian coordinates (r, t) for the case of one-dimensional motion with uniaxial deformation have the form

$$\begin{gathered}
(\rho_0/\rho)\,\partial\rho_1/\partial t + \rho_1\partial v/\partial r + (\rho_0/\rho)I_{12} = 0,\\
(\rho_0/\rho)\,\partial\rho_2/\partial t + \rho_2\partial v/\partial r - (\rho_0/\rho)I_{12} = 0\\
(\rho_i = \rho_i^0\alpha_i,\ \alpha_1 + \alpha_2 = 1,\ \rho = \rho_1 + \rho_2,\ i = 1, 2),\\
\rho_0\partial v/\partial t = \partial\sigma^{11}/\partial r,\\
\rho_0/\rho\,[\rho_1\partial e_1/\partial t + \rho_2\partial e_2/\partial t + (e_2 - e_1)\,I_{12}] = \sigma^{11}\partial v/\partial r,\\
\sigma^{11} = -p + \tau^{11},\ p = p_1(\rho_1^0, T) = p_2(\rho_2^0, T),\\
d\tau^{11}/dt = (4/3)\,\mu\,(\rho_0/\rho)\,dv/\partial r,\quad \tau^{11} \leqslant \tau^*,
\end{gathered} \tag{1.1}$$

where ρ_i, ρ_i^0, α_i, e_i are the mean density, true density, volume content, and specific internal energy of the i-th phase; ρ, v, T are the density, velocity, and temperature; σ^{11}, τ^{11}, p are the stress tensor, stress deviator, and hydrostatic pressure in the medium; μ, τ^* are the shear modulus and elastic limit, for the description of which Mises creep conditions will be used; I_{12} is the velocity of phase transitions for which the following relationships are fulfilled: $I_{12} = j_{12} - j_{21}$; for the $2 \rightarrow 1$ transition $j_{12} = 0$, $j_{21} > 0$; for the $1 \rightarrow 2$ transition $j_{12} > 0$, $j_{21} = 0$; if there are no phase transitions $j_{12} = 0$, $j_{21} = 0$.

The intensity of the phase transitions considered is greater, the more the pressure p exceeds the phase-transition pressure $p_S(T)$, i.e., the greater the nonequilibrium. Kinetics leading to retardation of phase transition and achievement of metastable states occur in the case of the transition $Fe^{\alpha} \rightleftharpoons Fe^{\varepsilon}$. We will assume [5-7] that the phase-transition velocity depends on the difference of the phase thermodynamic potentials (for identical pressures and temperatures) and on the volume content of the original phase. Moreover, we allow saturation of phase-transition velocity for sufficiently great deviations from the equilibrium line. Then at

Ufa. Moscow. Translated from Zhurnal Prikladnoi Mekhaniki i Tekhnicheskoi Fiziki, No. 5, pp. 128-135, September-October, 1976. Original article submitted October 12, 1975.

$j_{12} > 0$ or $j_{21} > 0$ the following relationships are realized:

$$j_{12} = \alpha_1 j_{12}^0 \left\{1 - \exp\left[-\left(\frac{p - p_s}{\Delta_{12}}\right)^{n_{12}}\right]\right\};$$
$$j_{21} = \alpha_2 j_{21}^0 \left\{1 - \exp\left[-\left(\frac{p_s - p}{\Delta_{21}}\right)^{n_{21}}\right]\right\}, \quad (1.2)$$

where the maximum phase-transition velocities are determined by the quantities j_{12}^0 and j_{21}^0. In contrast to [5-7], we consider here that at fixed pressure the transition i→j occurs the more rapidly, the greater the content of the original i-th phase.

The iron phase equilibrium curve in the region of the $\alpha \rightleftharpoons \varepsilon$ transition, obtained by Kaufman on the basis of static and dynamic data [8], may be approximated by the function

$$p_s(T) = K_1 + K_2 T/T_0 + K_3 (T/T_0)^2.$$

The kinetic relationships of Eq. (1.2) give the actual phase-transition hysteresis, determined experimentally, for example, in [3].

The equations of state and internal energy of the materials studied are represented in the form of three components, which describe elastic properties of the cold body in hydrostatic compression, harmonic oscillations of atoms in the lattice, and thermal excitation of electrons together with anharmonic effects of atomic oscillations:

$$p(\rho^0, T) = p_p + p_T + p_{ea}; \quad E(\rho^0, T) = e_p + e_T + e_{ea}.$$

In [9], defining $p_p(\rho^0)$ and $e_p(\rho^0)$, it was proposed that the Born–Mayer potential be used:

$$p_p(\rho^0) = Ax^{-2/3} \exp\left[b\left(1 - x^{1/3}\right)\right] - Kx^{-4/3}, \; x = \rho_0^0/\rho^0;$$
$$e_p(\rho^0) = 3Ab^{-1}\rho_0^{0-1} \exp\left[b\left(1 - x^{1/3}\right)\right] - 3K\rho_0^{0-1}x^{-1/3}.$$

Unfortunately, the coefficients A, b, K obtained in [9] for one and the same material vary markedly depending on which experimental results are processed: static, dynamic, or static and dynamic together. In numerical calculation in the pressure range to 1 Mbar it is expedient to use the simpler approximation

$$p_p(\rho^0) = b_1(1 - x) + b_2(1 - x)^2 + b_3(1 - x)^3;$$
$$e_p(\rho^0) = \rho_0^{0-1}(1 - x)\left[\frac{b_1}{2}(1 - x) + \frac{b_2}{3}(1 - x)^2 + \frac{b_3}{4}(1 - x)^3\right],$$

which allows accurate fixation of the hydrodynamic velocity of sound at the point $\rho^0 = \rho_0^0$ and significantly decreases the volume of calculations with no loss in accuracy.

The thermal components have the form

$$p_T = \gamma_T(\rho^0)\rho^0 e_T, \; e_T = c_v T,$$

where $\gamma_T(\rho^0)$ is the Grüneisen coefficient [9]; c_v is the atomic specific heat. The terms p_{ea} and e_{ea} related to thermal excitation of electrons and anharmonic effects of thermal motion of atoms in the lattice become significant at high pressures and temperatures ($p > 1$ mbar, $T > 10{,}000°K$) and therefore will not be considered.

§2. Using the model of a two-phase elastoplastic medium the problem of planar collision of a plate of thickness l_1 with a target of thickness $l - l_1$ will be solved numerically (the striker and target having infinite transverse dimensions). The initial state and boundary conditions of the striker–target system are known.

The physicochemical processes occurring upon shock-wave propagation in the target and striker lead to the development of a multiwave flow picture, in the course of which discontinuities (shock waves) are generated, interact, and degenerate. Therefore we use an indirect method of calculation employing pseudoviscosity, which allows calculation of the entire flow region in a single manner. In constructing the difference system [6] by the straight-line method (or particle method) the partial derivatives with respect to r at each time layer are approximated by a central divided difference (to second-order accuracy). This transforms the system of differential equations of Eq. (1.1) with partial derivatives with respect to r and t to a system of 6N (where N is the number of particles into which the computation region over r is divided) ordinary differential-difference equations in t, for all functions of which initial conditions at the moment of collision $t = 0$ are known. To solve the Cauchy problem obtained in this manner a modified Euler method is used. In the program developed a larger number of particles is realized than in [5] ($N = 184$). This permitted more accurate calcu-

lation of the processes occurring, including, which is most important, phase transitions. In the difference equation system, pseudoviscosity (linear and quadratic) is introduced, with consideration of which the stress tensor (at the j-th point of the time layer) appears as

$$\sigma^{11} = -p + \tau^{11} - \varphi,$$

while the pseudoviscosity is

$$\varphi = \rho_0 \Delta r (dv/dr)(c_1 a_0 + c_2 \Delta r |dv/dr|),$$

where c_1 and c_2 are the weights of the linear and quadratic pseudoviscosities. To increase accuracy of calculations in the rarefaction region we set $\varphi = 0$.

In realizing the difference system directly on the computer a portion of the calculations was performed with differing pseudoviscosity structures (including the differential analyzer of [10]), in order to reduce the width of the transition zone to 3-5 particles.

§3. According to the results of [1-7] a shock wave in an elastoplastic medium with phase transitions in the case of sufficiently high loading ($p > p_s$) has a three-wave configuration in both the compression stage and the rarefaction stage. Figure 1 shows an idealized profile of such a shock wave in the form of the pressure curve at some moment in time, where *ab* is the elastic precursor; D_e is the velocity of the elastic precursor; bc is the first plastic wave (bringing the original phase into a nonequilibrium state), propagating with velocity D_1; cd is the second plastic wave or phase transition wave, propagating with velocity D_{12}; ef is the elastic rarefaction wave; fg is the plastic rarefaction wave, bringing the second phase into a nonequilibrium state; gh is the rarefaction wave in which reverse phase transition occurs; and C_e, C_1, C_{21} are the corresponding velocities of rarefaction waves. We note that at pressures $p > 320$ kbar the waves bc and cd have identical velocities and so, without dividing, move together in the form of a single discontinuity bd (denoted by the dashed line) until the pressure decreases below 320 kbar under the influence of unloading. The multiwave character of the shock wave leads to the unloading wave "swallowing" the compression wave by stages: first the phase transition wave, then the first plastic wave, and finally, the elastic precursor.

In [3] shock-wave pressure profiles were obtained experimentally in Armco iron and Type 3 steel, which showed a multiwave configuration. The shock wave was induced by collision with an aluminum plate. The pressure profiles were determined by manganin sensors in the form of a double bifilar loop at various depths in the target from the collision surface. In the first series of experiments the aluminum striker had a thickness of 1 mm and collided with a Type 3 steel target (collision velocity not measured). In the second series of experiments the 7-mm-thick aluminum plate collided at a velocity of 2.11 ± 0.07 km/sec with a target of Armco iron or Type 3 steel. Two series of calculations were also performed for the experimental conditions of [3]. In the first series of calculations the striker velocity was estimated at 3.5 km/sec and in the second, at 2.11 km/sec. In all calculations the target material was Armco iron. We note that calculated and experimental data will also be compared in cases where in the computations the target material was Armco iron and the experiments used Type 3 steel (these materials have similar physicochemical properties).

Shock-wave motion calculations were also performed for an experiment [4] in which the velocity profile of the free surface of the iron target (target thickness 3.11 mm) was obtained with high accuracy by a light interferometer. The shock was initiated by a plate of tungsten carbide with collision pressure of 170 kbar.

In [6, 7] transition kinetics were determined from the thickness of the constant hardening zone in an iron specimen in which complete phase transition occurred. The experimental pressure profiles obtained in [3] and the free surface velocity profile of [4] permitted using the width and amplitude of the phase transition wave at various depths in the iron target to perform a number of calculations to more accurately determine the kinetics of phase transitions. As a result of these calculations values were found for the kinetic parameters appearing in Eq. (1.2) which agree best with the experiments of [3, 4]:

$$\begin{aligned} j_{12}^0 &= 6{,}6 \cdot 10^{10}\ \text{kg/m}^3\text{sec},\ \Delta_{12} = 24\ \text{kbar},\ n_{12} = 3, \\ j_{21}^0 &= 3{,}7 \cdot 10^{11}\ \text{kg/m}^3\text{sec},\ \Delta_{21} = 24\ \text{kbar},\ n_{21} = 3. \end{aligned} \tag{3.1}$$

On the whole, Eqs. (1.2), (3.1) define more intense kinetics for phase transitions in iron than the data of [6, 7] indicate.

Figure 2 presents calculated results in the form of pressure curves for striker and target (first series) at various moments after collision. The point K corresponds to the contact surface, dividing striker and target. At the initial moment the shock-wave pressure reaches 560 kbar, so that the first and second plastic waves move with identical velocity $D_1 = 6.1$ km/sec, which then decreases with decrease in pressure, while at dis-

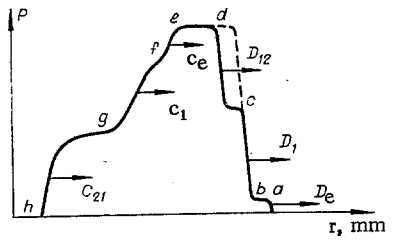

Fig. 1

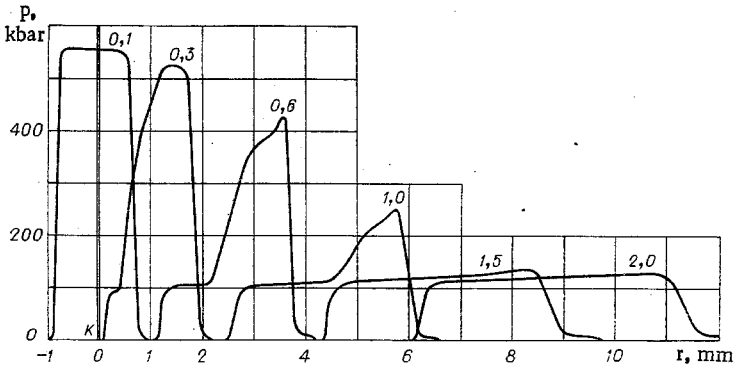

Fig. 2

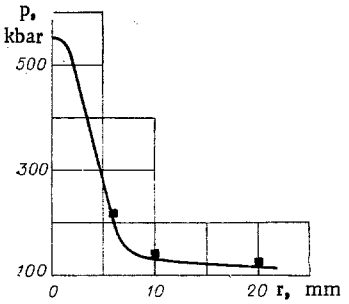

Fig. 3

tances of 5-6 mm, division of the shock wave into D_1 and D_{12} commences. The rarefaction wave, formed over a very brief time (due to the low thickness of the striker $l_1 = 1$ mm), rapidly begins to "swallow" the shock wave: first the wave in which phase transition is realized, then the first plastic wave.

Figure 3 shows good agreement for the first series between calculated (solid line) and experimental (points from [3]) pressure damping over target depth. Intense shock-wave damping is completed at a depth of 7 mm, i.e., in the region where phase transition occurs, so that study of the process at distances up to 7 mm is of greater interest than at 10 and 20 mm, where slow damping of the first plastic wave occurs.

Pressure curves at various moments, obtained in calculations for the second series, are presented in Fig. 4. At the moment of collision the original target phase completely absorbs the load, and only after the passage of a certain time does transition into the second phase occur, leading to relaxation unloading. Formation of a multiwave structure in striker and target appears more clearly here than in the first series. The pressure curve at $t = 3.0$ μsec is marked with letters. In the numerical computation with pseudoviscosity the segment bc has finite thickness, while the width of zone cd is determined by the phase-transition kinetics.

Calculated pressure profiles for the shock wave over time for the first and second series of experiments are shown by the solid line in Figs. 5 and 6, while the dashed lines indicate the experimental pressure profiles of [3] at the same target sections. For the first series, curves 1-3 were obtained at depths of 6, 10, and 20 mm; for the second series, curves 1-4 are at 4, 11, 12, and 17 mm.

In these experiments the moment of collision was not measured directly, so that oscillograms were produced in coordinates (p, t) using the measured velocity of the first plastic wave $D_1 = 5.05 \pm 0.07$ km/sec, which corresponds to a pressure on the shock front of 130 kbar. But the velocity D_1 of plastic wave bc at the initial moment of time is determined by the collision pressure and under the given conditions is greater than 5.05 km/sec. Then as shock-wave formation proceeds, D_1 decreases. It is this fact which causes the calculated pressure profiles at fixed target sections in the first and second series to lead the oscillograms processed in such a manner at the same target sections. Thus the data presented in [3] are shifted along the time axis t by some amount τ. For the first series $\tau_1 = 0.21$, $\tau_2 = 0.28$, $\tau_3 = 0.43$; for the second $\tau_1 = 0.15$, $\tau_2 = 0.17$, $\tau_3 = 0.18$, $\tau_4 = 0.22$, (τ, μsec; subscript denotes corresponding curve number in Figs. 5 and 6). In the numerical calculation of the experiment of [4], in which the moment of collision was measured, the calculated exit time of the shock wave onto the free surface coincided with experiment with great accuracy.

As is evident from Figs. 5 and 6 the calculated pressure profiles at high target depths are somewhat wider than the experimental ones. This may evidently be explained by the fact that the calculations modelled

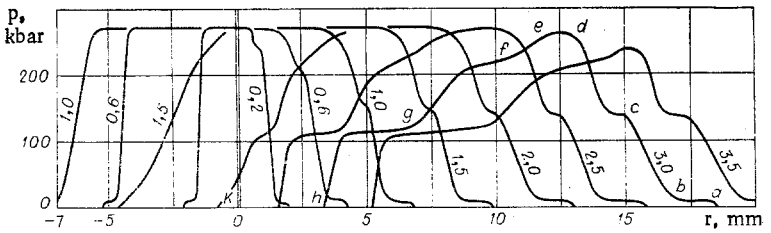

Fig. 4

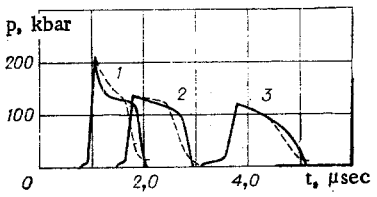

Fig. 5

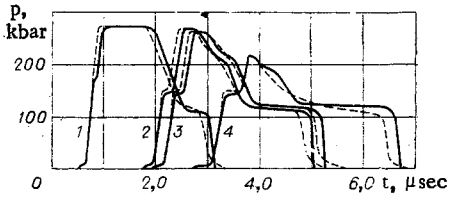

Fig. 6

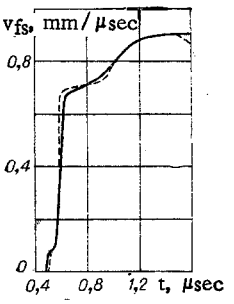

Fig. 7

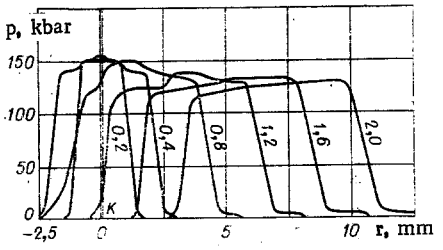

Fig. 8

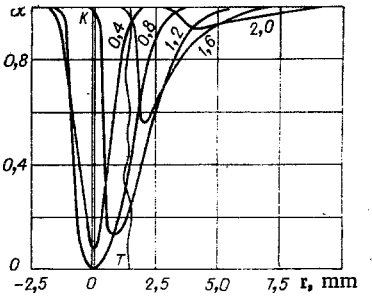

Fig. 9

a purely planar shock (with infinite transverse dimensions), while in the experiments, at later times, two-dimensional effects caused by lateral unloading begin to appear, since at the moment of collision the planar segment comprised 60-65 mm.

We will consider one more important fact concerning the second series of experiments. The calculations show that in these experiments phase transitions in the target occurring at the shock front should exist at distances less than 4 mm from the collision surface. However, in the experimental profile obtained at a depth of 4 mm (dashed line 1, Fig. 6) the phase-transition wave is not distinguishable. This is evidently related to insufficient experimental resolution, since if phase transitions did not occur, the pressure at the shock front at this point would be somewhat higher than the corresponding pressure at depths of 11 and 12 mm (curves 2 and 3, Fig. 6). Calculations performed solely for the first phase of iron show that the disagreement should be ~18 kbar. From this viewpoint, the velocity profile of the free surface of the iron target [4] is of great interest. At a collision pressure of 170 kbar for a target thickness of 3.11 mm a clear three-wave profile was obtained, indicating that phase transitions occur in the iron at these depths. Accurate determination of the collision moment in [4] allowed evaluation of the mean velocity of the first shock plastic wave at a given target thickness. This value proved equal to ~5.3 km/sec. The calculated values and experimental data (solid and dashed lines, respectively) presented in Fig. 7 indicate the high accuracy of the calculations.

Thus, the numerical calculations of shock waves with phase transitions and analysis of the experiments of [3, 4] provide a basis for concluding that the divergence of the experimental curve from the calculations at a depth of 4 mm (see Fig. 6) is produced by insufficient resolution in the measurements. This is supported by the fact that at these distances the thickness of the phase-transition front is comparable to the thickness of the manganin sensor.

§4. Experiments on iron hardening in low-carbon steel (at pressures of the order of 130 kbar and higher) showed the high effectiveness of shock-wave processing in comparison to other methods of hardening (for ex-

ample, cold rolling). The high sensitivity of iron and steel to significant hardening in shock waves is caused by phase transitions occurring in the specimen tested. In [6, 7] calculations of shock-wave motion were made and experiments on iron hardening with a planar shock of striker on target were performed. Comparison of calculated data with experimentally measured penetration depth of constant hardening allowed evaluation of the real velocity of the $\alpha \rightarrow \varepsilon$ transitions. It developed that the velocity of the reverse transition was an order higher than that of the forward one. This has been confirmed in the present calculations.

The kinetic parameter values obtained above [Eq. (3.1)] were used for calculation of shock waves of various intensities (striker velocity was varied), developing as a result of collision of an iron plate with an iron target [6, 7]. The calculations showed that the experimentally measured depth of the constant-hardening zone was reduced due to specimen shrinkage caused by lateral expansion upon lateral unloading. In these hardening experiments the shrinkage comprised 2 to 5 mm and must be considered in comparing calculations with experiment. Such a comparison must be considered separately.

We will consider one more experiment [11] on hardening of low-carbon steel, in which planar collision of a 2.5-mm-thick plate (collision pressure 155 kbar) was produced, leading to phase transitions in a shock wave. Calculations performed for these conditions ($v_0 = 900$ m/sec) for striker and target at various moments of time are shown in Figs. 8 and 9, where it is evident that the depth of the complete phase-transition zone is of the order of 0.5 mm. This is caused by the fact that the pressure on the shock front (initially somewhat exceeding the phase-transition pressure) falls because of both the phase transitions, which have commenced, and the overtaking rarefaction wave. At a depth of 2-3 mm, phase transitions in the target do not go to completion, and at 10-15 mm they cease entirely. Thus it may be expected that in the given case within the shock wave there occurs a relatively small increase in hardness in layers closest to the collision surface. Experiment gives the same result (increase in specimen hardness by only 20% at an initial microhardness of 130 HV), since, in practice, because of technological difficulties hardness measurement takes place at some depth below the surface (denoted by point T in Fig. 9), i.e., at a point where phase transitions do not go to completion. Thus, this experimental fact does not contradict the concept of the relationship between $Fe^{\alpha} \rightleftharpoons Fe^{\varepsilon}$ transitions and explosive hardening.

LITERATURE CITED

1. L. V. Al'tshuler, "Use of shock waves in high-pressure physics," Usp. Fiz. Nauk, 85, No. 2 (1965).
2. S. A. Novikov, I. I. Divnov, and A. G. Ivanov, "Shock-compression wave structure in iron and steel," Zh. Éksp. Teor. Fiz., 47, No. 3 (1964).
3. A. V. Anan'in, A. N. Dremin, and G. I. Kanel', "Structure of shock waves and rarefaction waves in iron," Fiz. Goreniya Vzyva, 9, No. 3 (1973).
4. L. M. Barker and R. E. Hollenbach, "Laser interferometer for measuring high velocities of any reflecting surface," J. Appl. Phys., 43, No. 11 (1972).
5. R. I. Nigmatulin, "A model of motion and shock waves in two-phase solids with phase transitions," Zh. Prikl. Mekh. Tekh. Fiz., No. 1 (1970).
6. R. I. Nigmatulin, N. F. Skugorova, and N. N. Kholin, Waves in Continuous Media. Nonstationary Shock Waves and Hardening [in Russian], Report No. 1081, Inst. Mekh. Mosk. Gos. Univ. (1970).
7. S. S. Grigoryan, K. I. Kozorezov, R. I. Nigmatulin, N. F. Skugorova, and N. N. Kholin, "Nonsteady shock waves in metals with phase transitions and hardening by explosion," Astronaut. Acta, 17, (1972).
8. L. Kaufman, "Phase equilibria and transitions in metals under pressure," in: Solids under High Pressure [Russian translation], Mir, Moscow (1968).
9. V. N. Zharkov and V. A. Kalinin, The Equation of State of Solids at High Pressures and Temperatures [in Russian], Nauka, Moscow (1968).
10. A. I. Ivandaev, "A method of introducing 'pseudoviscosity' and its application in refining difference solutions of the hydrodynamic equations," Zh. Vychisl. Mat. Mat. Fiz., 15, No. 2 (1975).
11. A. A. Deribas, Physics of Hardening and Welding by Explosion [in Russian], Nauka, Moscow (1972).